Local structure of $CuIn_3Se_5$: X-ray absorption fine structure study and first-principles calculations

C.-H. Chang,[1,*] Su-Huai Wei,[2] J. W. Johnson,[3] S. B. Zhang,[2] N. Leyarovska,[4] Grant Bunker,[5] and T. J. Anderson[3]
[1]*Department of Chemical Engineering, Oregon State University, Corvallis, Oregon 97331, USA*
[2]*National Renewable Energy Laboratory, Golden, Colorado 80401, USA*
[3]*Department of Chemical Engineering, University of Florida, Gainesville, Florida 32611, USA*
[4]*Advanced Photon Source, Argonne National Laboratory, Argonne, Illinois 60439, USA*
[5]*Department of Physics, Illinois Institute of Technology, Chicago, Illinois 60616, USA*
(Received 12 February 2003; published 20 August 2003)

A detailed extended x-ray absorption fine structure (EXAFS) study of $CuInSe_2$ and $CuIn_3Se_5$ on Cu-*K*, In-*K*, and Se-*K* edges was performed. It was found that $CuInSe_2$ and $CuIn_3Se_5$ have well-defined local structure with the same average Cu-Se and In-Se bond lengths. They can be best described by structures containing weighted local tetrahedral cationic clusters around each Se: $2Cu+2In$ ($k=8$), and equal number of $V_{Cu}+Cu+2In$ ($k=7$) and $V_{Cu}+3In$ ($k=9$), where k denotes the nominal number of valence electrons of the cation clusters. $CuInSe_2$ consists of 100% $k=8$ clusters and $CuIn_3Se_5$ consists of 20% $k=8$ and 40% $k=7$ and 40% $k=9$ clusters. First-principles band structure calculations of various $CuInSe_2$, $CuIn_3Se_5$ and $CuIn_5Se_8$ compounds confirmed that the average Cu-Se and In-Se bond lengths in various ordered vacancy structures are identical to within the calculation uncertainty, in agreement with the present EXAFS measurements. The first-principles calculations also find that the formation energy of several possible crystal structures for $CuIn_3Se_5$ and $CuIn_5Se_8$ are very similar, which explains why the long-range order of $CuIn_3Se_5$ is not uniquely determined.

DOI: 10.1103/PhysRevB.68.054108 PACS number(s): 61.10.Ht, 71.20.Nr, 61.14.Lj

I. INTRODUCTION

Photovoltaic devices based on $CuInSe_2$ and related compounds have developed rapidly in the last few years, achieving high active area efficiencies 18.8% in small device.[1] The observed junction between α-$CuInSe_2$ and the In-rich compounds (e.g., $CuIn_3Se_5$) appears to play an important role in the process.[2] Many works have been carried out to investigate the structure of this compound. A review of the reported structural studies of this compound is given in Table I. Palatnik and Rogacheva[3] first reported $CuIn_3Se_5$ compound and assigned the crystal structure to space group of either $I\bar{4}$ or $I\bar{4}2m$ based on the observed extinction rule from x-ray powder diffraction data. Later, a refined structure solution was given by Hönle *et al.*[4] using single crystal x-ray diffraction data. They determined the space group $P\bar{4}2c$ and proposed the name, *P*-chalcopyrite, for this phase. Tseng and Wert[5] proposed a vacancy-ordered structure model, with $I\bar{4}$ symmetry, from transmission electron diffraction data. The proposed structure model, however, has stoichiometry of Cu:In:Se=1:5:8 rather than 1:3:5. Xiao *et al.*[6] studied the epitaxial $CuIn_3Se_5$ thin film by transmission electron microscope. They constructed a structure model by introducing ordered point defects into chalcopyrite $CuInSe_2$ structure to account for the extra diffraction spots. They further suggested $CuIn_3Se_5$ is an ordered defect chalcopyrite structure. Nomura and Endo[7] also constructed a structure model for $CuIn_3Se_5$ from the same principle. Their model is not an ordered vacancy compound (OVC) although they referred it as an OVC in the paper. Hanada *et al.*[8] investigated the crystal structure of $CuIn_3Se_5$ by combination of electron and x-ray diffraction. They limited the space group to $I\bar{4}$ or $I\bar{4}2m$ based on the observed extinction rule followed by powder x-ray data. They further determined the space group to be $I\bar{4}2m$ from a convergent electron diffraction pattern along the [001] zone axis. They proposed a structure model $ABIn_2Se_4$ for $CuIn_3Se_5$, which is represented by $(Cu_{0.8}\mathbf{V}_{0.2})(In_{0.4}\mathbf{V}_{0.6})In_2Se_4$ ($\mathbf{V}$ denotes structure vacancy). It is clear from their structure model (Fig. 9) that the vacancy is randomly distributed in $2a$ and $2b$ sites along with Cu and In atoms. They concluded that $CuIn_3Se_5$ is neither an OVC nor a defect chalcopyrite structure. More recently, Merino *et al.*[9] refined the $CuIn_3Se_5$ structure using the structural models proposed by Hönle *et al.*[4] and Hanada *et al.*[8] based on their powder x-ray diffraction (XRD) data. They suggested the model proposed by Hönle *et al.*[4] is more reliable based on the argument that more realistic interatomic distances could be derived from the Rietveld refinement.

Zhang and co-workers[10,11] proposed an ordered vacancy compound structure model based on the first-principles total energy calculations. Their model suggests that the OVC is stabilized by the formation of $(2\mathbf{V}_{Cu}^{-}+\mathbf{In}_{Cu}^{+})$ defect pairs in a perfect $CuInSe_2$ crystal. It has a weighted distribution of three types of local tetrahedral around each Se: $2Cu+2In$ (denoted as $k=8$), $V_{Cu}+Cu+2In$ (denoted as $k=7$), and $V_{Cu}+3In$ (denoted as $k=9$). Here k is the sum of valence electrons of Se-centered nearest neighbor cations. The $k=7$ and 9 clusters occur in pairs and is close to each other to enhance the mutual Coulomb attractions. Therefore, $CuIn_3Se_5$ can be described as having 20% of the $k=8$ cluster, and 40% each of the $k=7$ and 9 clusters.

The determination of the crystal structure of $CuIn_3Se_5$ is also complicated by different techniques used in the characterization. The questions in single crystal x-ray structure determination are whether a true single crystal was used and

TABLE I. Reported structure data for $CuIn_3Se_5$.

Crystallographic data	Structure determination method	OVC?	References
$I\bar{4}$ or $I\bar{4}2m$ $a=5.75$ Å, $c=11.50$ Å	Powder XRD	-	3
$P\bar{4}2c$ $a=5.755$ Å, $c=11.52$ Å	Single crystal XRD full matrix structure refinement	No	4
$I\bar{4}$	selected area electron diffraction (SAD)	Yes	5
-	SAD and high resolution electron microscopy (HREM)	Yes	6
Tetragonal	Powder XRD	No	7
$I\bar{4}2m$ $a=5.754$ Å, $c=11.518$ Å	Powder XRD, SAD, convergent beam electron diffraction (CBED)	No	8
$P\bar{4}2c$ $a=5.7555$ Å, $c=11.5303$ Å	Powder XRD Rietveld refinement	No	9

the limitation in unique determination of the space group. Transmission electron microcopy is capable of choosing a single crystal to study. However, the intensity data are not easy to utilize. Although the observed transmission electron diffraction (TED) patterns in Tseng and Wert[5] and Xiao *et al.*[6] can be explained qualitatively by their proposed ordered vacancy structure models, their structure models can not be uniquely determined from the observed TED patterns and the intensity data were not used quantitatively.

To shed some light on this issue, we have studied the local structure of $CuIn_3Se_5$ using the extended x-ray absorption fine structure (EXAFS) measurement performed on the Cu, In and Se *K* edges. The first-principles total energy calculations were also performed to compare with experimental data.

II. EXPERIMENTAL METHODS

A. Sample preparation

The samples were prepared from powder Cu_2Se and In_2Se_3 in boron nitride (BN) coated evacuated fused silica ampoules. The BN coating was used to prevent copper devitrification of the fused silica at high temperature.[12] These mixtures were then slowly heated to the melting temperature then gradually cooled to 700 °C, and were kept in furnace at 700 °C for a week to assure equilibrium. It is then quenched in liquid nitrogen. Powder XRD and wavelength dispersive x-ray spectroscopy were used to verify the formation of desired homogeneous single-phase materials.

B. EXAFS measurements and data reduction

The EXAFS specimens were prepared by grinding the synthesized polycrystalline material. The particle size distribution was characterized using a Horiba Capa-700 particle analyzer, which confirmed particles were less than ten microns in diameter with average particle size of 4 μm. The sizes of these particles are smaller than the absorption length of $CuInSe_2$ at the Cu-*K* edge. The fine powder was spread over a transparent tape, taking care to uniformly distribute the powder and avoid pinholes. Same measurements were taken with samples of one and two layers of tapes to further test the influence of film thickness on the EXAFS spectra through self-absorption. No distortion was observed on the amplitude of the EXAFS spectra taken from these measurements. The EXAFS measurements were performed on the Materials Research Collaborative Access Team beamline of the Advanced Photon Source (APS) at Argonne National Laboratory, which uses an APS undulator *A*. The beamline optics incorporates a Si(111) double crystal monochromator, and a Rh coated harmonic-rejection mirror, which was set to reject the second and higher order harmonics. The x-ray intensities were monitored using x-ray ionization chambers. Detector linearity was verified by attenuating the primary beam. The room temperature EXAFS spectra were measured in the transmission mode.

C. Data analysis

The collected data were analyzed by standard procedure[13] using the WINXAS package.[14] The experimental intensity data were first converted to absorption coefficient based on $\mu(E)x=\ln(I_0/I)$, where μ is x-ray absorption coefficient, E is the x-ray photon energy, x is the sample thickness, and I_0 and I are the intensities of the incident and transmitted beams, respectively. The resulted absorption spectra were then subject to pre-edge background removal. A typical Cu *K*-edge spectrum of $CuInSe_2$ is shown in Fig. 1(a). The next step was to convert the photon energy E to the photoelectron wave vector $\mathbf{k}$ via $\mathbf{k}=\sqrt{2m(E-E_0)/\hbar^2}$, where m is the electron mass, and E_0 is the *K*-edge energy. The normalized XAFS spectra were obtained by subtracting the background $\mu_0(k)$ from the measured absorption coefficient $\mu(k)$ and were normalized by the edge jump $\Delta\mu_0(0)$:

$$\chi(k)=\frac{\mu(k)-\mu_0(k)}{\Delta\mu_0(0)}. \tag{1}$$

The resulting $\chi(k)$ oscillations, shown in Fig. 1(b), were then Fourier transformed into R space. The Fourier-transformed (FT) Cu-*K* edge *R*-space data are shown in Fig. 1(c). A square window was used to isolate the first-nearest-

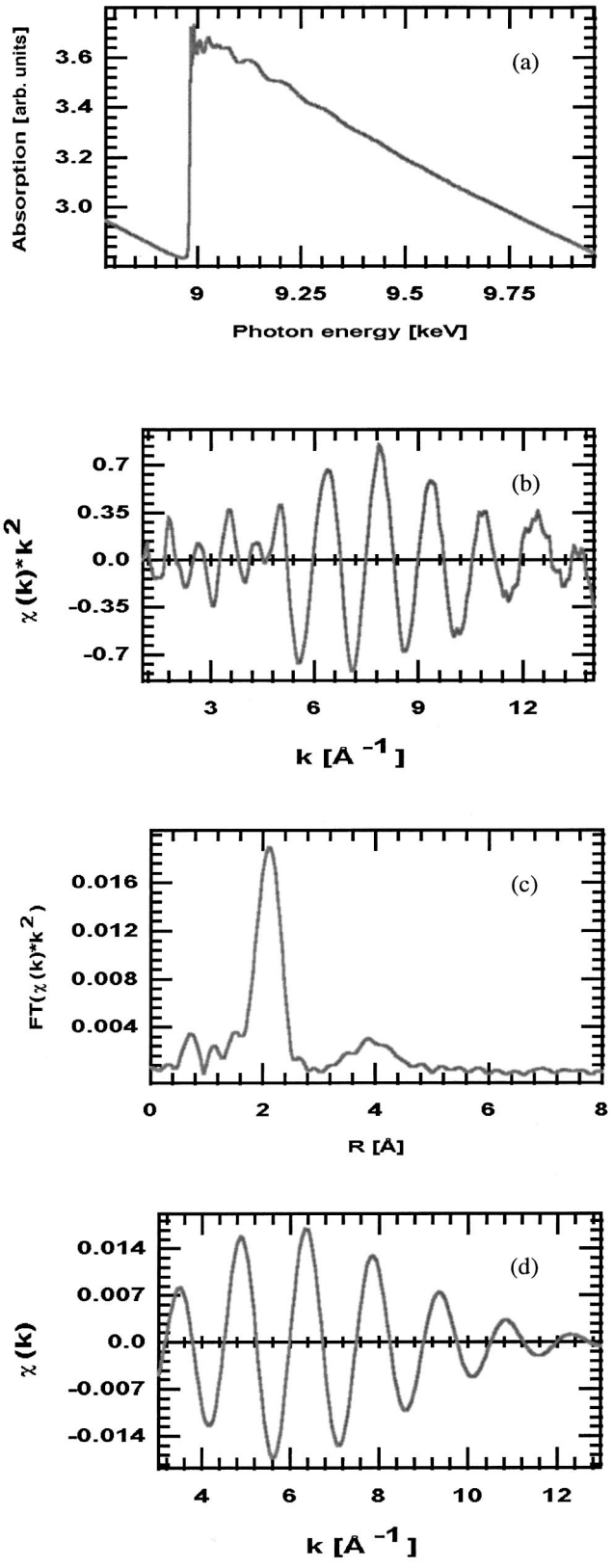

FIG. 1. (a) Absorption as a function of photon energy at the Cu K edge in $CuInSe_2$ at 298 K. (b) Cu K-edge EXAFS oscillations, $k^2\chi(k)$, as a function of k after background removal. (c) Fourier transform of (b) to real space. The transform window is 3–12 $Å^{-1}$. (d) Fourier filtered first shell EXAFS data.

neighbor FT peak for inverse Fourier transforms. The analysis was not sensitive to types of windows when we analyzed the standard compound and the unknown under exactly the same conditions. The resulting first shell EXAFS spectrum is shown in Fig. 1(d). The same k- and R-space windows were applied to the data analysis for the spectra of $CuInSe_2$ and $CuIn_3Se_5$.

The standard EXAFS equation was used[13] to obtain quantitative information in the least square analysis;

$$\chi(k)=\sum_j N_j A_j(k)\sin[2kR_j+\delta(k)]. \tag{2}$$

$A_j(k)$ is the amplitude function, which is expressed as

$$A_j(k)=\frac{1}{kR_j^2}S_0^2F_j(k)\exp(-2k^2\sigma_j^2)\exp\left(\frac{-2R_j}{\lambda(k)}\right). \tag{3}$$

Variables in Eqs. (2) and (3) include N_j, the number of atoms in jth shell; R_j, the mean distance between the absorbing atom and the jth shell; $F_j(k)$, the magnitude of the backscattering amplitude of the jth neighbor atom; $\delta_j(k)$, the electronic phase shift due to the atomic potentials; and σ^2, the corresponding mean-square relative displacement. S_0 is the amplitude reduction factor representing central atom shake-up and shake-off effects, and $\lambda(k)$ is the photoelectron mean free path.

The amplitude function, $A_j(k)$, and phase shift, $\delta_j(k)$, for the Cu and In K edges were extracted from the $CuInSe_2$ spectra using the known structural data. The *ab initio* multiple-scattering code FEFF7 (Ref. 15) was used to calculate $F_j(k)$, $\delta_j(k)$, and $\lambda(k)$ for Se K-edge data analysis.

III. RESULTS

A. Cu local structure

The Cu-K edge EXAFS spectra and FT-R space data for $CuIn_3Se_5$ and $CuInSe_2$ are shown in Figs. 2(a) and 2(b). The first FT peak appears at about 2.1 Å is attributed to the scattering of first nearest neighbors (Se). The second broad peak around 3.9 Å arises from interaction with the second nearest neighbors (Cu, In). The isolated first shell spectra for $CuInSe_2$ and $CuIn_3Se_5$ are given in Fig. 2(c). It is clear that the two spectra are almost identical except the one for $CuIn_3Se_5$ has a slightly larger damping coefficient. This indicates the local structures (i.e., the bond length, $d_{\text{Cu-Se}}$, and the number of nearest neighbors, N) around the Cu atoms in these two semiconductor alloys are nearly the same. To obtain quantitative data a least squares fit to the standard EXAFS equation was performed.

Structural parameters of chalcopyrite $CuInSe_2$ are needed for obtaining the amplitude function, $A_j(k)$, and phase shift, $\delta_j(k)$, from the Cu K-edge $CuInSe_2$ EXAFS spectrum. A review of the reported structural data for chalcopyrite $CuInSe_2$ is listed in Table II. The agreement in cell parameters is good, but a considerable difference is observed in the reported Se atomic coordinate, $x(\text{Se})$, and the resulting bond lengths, $d_{\text{Cu-Se}}$ and $d_{\text{In-Se}}$. Merino *et al.*[20] have reported the Se atomic coordinate, $x(\text{Se})$, as well as the Cu-Se and In-Se

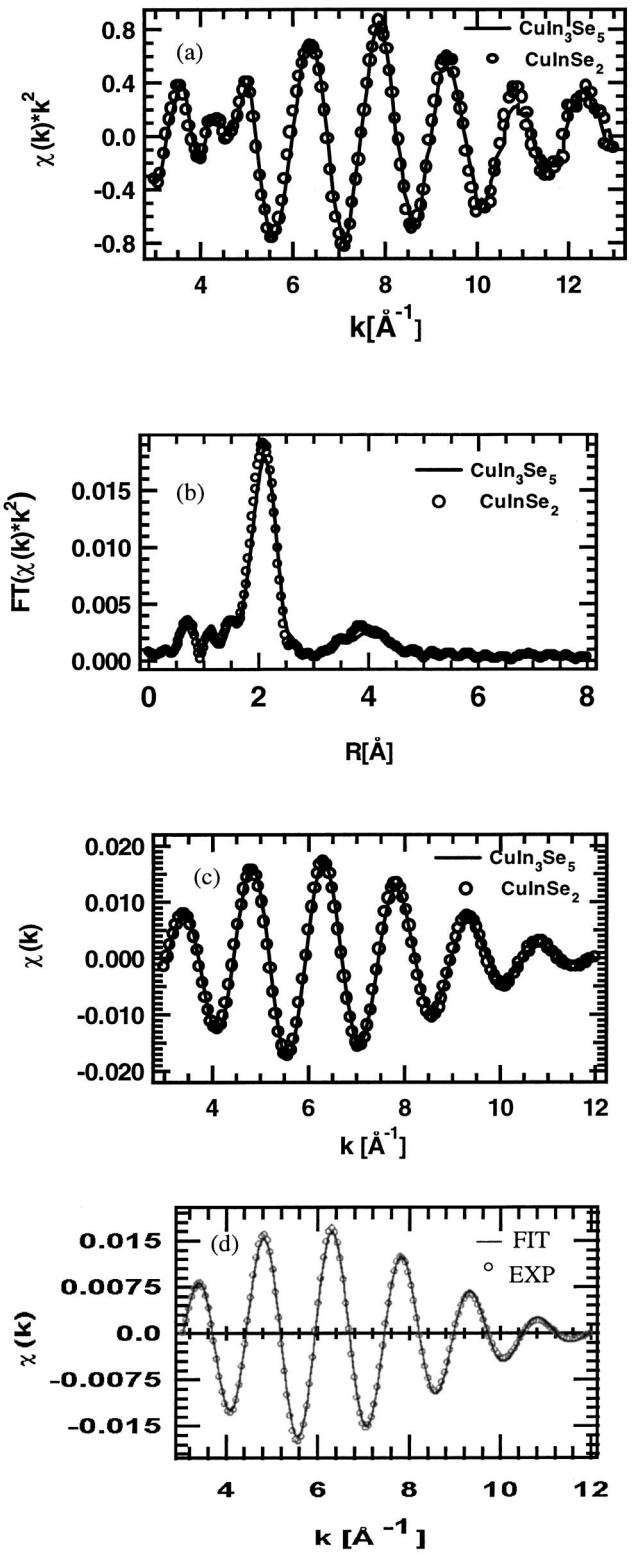

FIG. 2. The Cu-*K* edge data for $CuIn_3Se_5$ and $CuInSe_2$. (a) $k^2\chi(k)$ EXAFS spectra, (b) magnitudes of the Fourier transform, (c) Fourier filtered EXAFS for the first shell peaks, and (d) least-square fits to the Fourier-filtered first shell *k*-weighted $\chi(k)$. The data for $CuIn_3Se_5$ and reference $CuInSe_2$ were filtered over an identical range in *r* space, from 1.58 to 2.58 Å

inter-atomic distances depend on the Cu occupation number based on x-ray powder diffraction and Rietveld refinement. However, our EXAFS experimental results and first principle calculations do not support their model.[22] EXAFS measurements at the Cu *K* edge of slightly different compositions of nominally $CuInSe_2$ reveal that the Cu-Se interatomic distance is independent of the composition. The result is consistent with first-principles total energy calculations for this system. The calculations show the Cu-Se bond length is independent of the Cu occupation number while the In-Se bond length decreases only slightly when the Cu occupation decreases. Their observation could be well explained by partial disorder of Cu and In cation sites through the formation of short-range $CuInSe_2$ polytypes. Our previous results validate the use of chalcopyrite $CuInSe_2$ as a standard structural model for extracting amplitude function, $A_j(k)$, and phase shift, $\delta_j(k)$, from the $CuInSe_2$ EXAFS spectrum. The bond length values, $d_{\text{Cu-Se}}=2.424$ Å and $d_{\text{In-Se}}=2.598$ Å, from Spiess *et al.*[17] are adopted here for chalcopyrite $CuInSe_2$ structures. The least square fits of the *k*-weighted data at 298 K are shown in Fig. 2(d). The obtained structural parameters are given in Table III. The fitting results confirmed the Cu-Se interatomic distance is conserved between $CuInSe_2$ and $CuIn_3Se_5$ within an estimate uncertainty of 0.005 Å. The nearest neighbor coordination number for Cu is fixed at 4 for the least square fitting in both phases.

B. In local structure

The In *K*-edge FT-*R* space data for $CuIn_3Se_5$ and $CuInSe_2$ are given in Fig. 3(a). The first FT peak arises at 2.26 Å from the scattering of first nearest neighbors (Se). The isolated first shell spectra for $CuInSe_2$ and $CuIn_3Se_5$ are given in Fig. 3(b). The two spectra are almost identical. This indicates the first nearest neighbor environment (i.e., bond length $d_{\text{In-Se}}$ and number of nearest neighbors, *N*) around In atoms in these two semiconductor alloys are identical. The least square fits of the *k*-weighted data at 298 K are shown in Fig. 3(c). The fitted structural parameters are given in Table III. The fitting results confirmed the In-Se interatomic distance is conserved between $CuInSe_2$ and $CuIn_3Se_5$ within an estimate uncertainty of 0.005 Å. The nearest neighbor coordination number is fixed at 4 for the least square fitting.

C. Se local structure

The Se-*K* edge raw x-ray absorption data, $k^2\chi(k)$ spectra, and FT-*R* space data for $CuIn_3Se_5$ and $CuInSe_2$ are shown in Figs. 4(a) and 4(b). Unlike the Cu *K*-edge data, the first peak shows interference (with a shoulder). This interference is caused by the mixing of the two kind of nearest neighbors (Cu and In) surrounded the Se, as can be seen from the FEFF7 analysis. The Se-center tetrahedron of chalcopyrite $CuInSe_2$ consists of two Cu atoms and two In atoms around the central Se atom. Similarly, $CuIn_3Se_5$ can be described as a normal tetrahedral structure with 20% unoccupied cation tetrahedral sites. The first shell Se-*K* edge EXAFS data should reveal the number of nearest neighbors in the ratio of Cu:In:V_{Cu}=1:3:1, if $CuIn_3Se_5$ did belong to the defect-tetrahedral structural family.[23]

TABLE II. Structural parameters of $CuInSe_2$ determined by x-ray diffraction.

Type	a (Å)	c (Å)	u (Se)	$d_{\text{Cu-Se}}$ (Å)	$d_{\text{In-Se}}$ (Å)	Reference
Powder	5.782	11.620	0.235	2.484	2.586	16
Single crystal	5.784	11.616	0.224	2.424	2.598	17
Powder	5.784	11.614	0.2268	2.433	2.588	18
	5.781	11.609	0.2281	2.436	2.582	
	5.783	11.611	0.2227	2.420	2.602	
Single crystal	5.781	11.6422	0.2260	2.4337	2.5893	19
Powder	5.7799-	11.6172-	0.2277-	2.424-	2.596-	20
	5.7838	11.6263	0.2348	2.458	2.558	
Single crystal	5.731	11.513	0.2277	2.4139	2.5611	21

The isolated first shell spectra for $CuInSe_2$ and $CuIn_3Se_5$ are given in Fig. 4(c). The two spectra are very different in contrary to Cu-*K* and In-*K* edge spectra. The difference at lower k suggests a difference in the number of In and Cu nearest neighbors. There are two types of first nearest neighbors (Cu and In) around Se. The same data analysis procedures by using experimental standard compound could not be applied to analyze Se edge spectra. The *ab initio* multiple-scattering code FEFF7 (Ref. 15) was used for the calculation of $F_j(k)$, $\delta_j(k)$, and $\lambda(k)$ to obtain quantitative estimates of the number of nearest neighbors and their distances. The isolated first shell spectrum for $CuInSe_2$ and the least squares fit are given in Fig. 5(a). The fitting was performed by assuming the number of nearest neighbors (NN) Cu=2, NN In=2, and their distances $d_{\text{Cu-Se}}=2.424$ Å and $d_{\text{In-Se}}=2.598$ Å. Fitted results (Table IV) showed the Se-*K* edge data are consistent with the Cu and In *K*-edge data. It is not possible to de couple the values of the NN and S_0. To avoid this problem, the resulting reduction factor S_0^2 from the least square fitting of $CuInSe_2$ was retained and used in the analysis of Se *K*-edge spectrum for $CuIn_3Se_5$. The fitting was performed using NN Cu=0.8, NN In=2.4, $d_{\text{Cu-Se}}=2.424$ Å, and $d_{\text{In-Se}}=2.598$ Å. The FT filter first shell spectrum for $CuIn_3Se_5$ with the least square fit is shown in Fig. 5(b). The fitting results (Table IV) confirm that $CuIn_3Se_5$ does belong to the defect-tetrahedral structure, which is characterized by vacant tetrahedral site in the Se-centered tetrahedron. The data are consistent with the model proposed by Zhang *et al.*,[10] which suggested that the structure of $CuIn_3Se_5$ consists of three types of local tetrahedral cationic clusters around each Se: $V_{\text{Cu}}+\text{Cu}+2\text{In}$ ($k=7$), $2\text{Cu}+2\text{In}$ ($k=8$), and $V_{\text{Cu}}+3\text{In}$ ($k=9$).

D. First-principles calculation

We have also studied the local crystal structures of various $CuInSe_2$, $CuIn_3Se_5$, and $CuIn_5Se_8$ compounds using the first-principles band structure method.[24] To choose the crystal structures, we have followed the two guidelines: (a) The arrangement of atoms in these structures has minimal deviations from the octet rule, and (b) they have low Coulomb energy. For $CuInSe_2$ the three prototype structures that satisfy these conditions are shown in Fig. 6. Based on the arrangements of the cations, they are denoted as chalcopyrite (CH), CuAu-like (CA), and primitive (P) structures. All three $CuInSe_2$ structures have the same first nearest neighbor local structures for Cu, In, and Se. For $CuIn_5Se_8$, the six structures we have studied are shown in Fig. 7. A close look of the structures in Fig. 7 shows that these structures can be obtained from $CuInSe_2$ in Fig. 6 by having one ($2V_{\text{Cu}}+\text{In}_{\text{Cu}}$) defect pair in every 16-atom (4CuInSe_2) unit cell. For example, type-*A* and type-*B* $CuIn_5Se_8$ are derived from CA-$CuInSe_2$ (001), type-*C* $CuIn_5Se_8$ is derived from CA-$CuInSe_2$ (100), type-*D* and type-*E* $CuIn_5Se_8$ are derived from CH-$CuInSe_2$ by forming alternative Cu-V_{Cu}-In_{Cu}-V_{Cu}-Cu chains along the [110] and [001] directions, respectively, in the Cu sublattice, and type-*F* $CuIn_5Se_8$ is derived from P-$CuInSe_2$ by forming alternative Cu-V_{Cu}-In_{Cu}-V_{Cu}-Cu chains along the [001] direction in the Cu sublattice. The original $CuInSe_2$ structure can be easily noticed if one puts Cu back on the V_{Cu} sites and the In_{Cu} antisites. For $CuIn_3Se_5$, it can be constructed by adding one $CuInSe_2$ to one $CuIn_5Se_8$.

Our total energy calculations show that for $CuIn_5Se_8$, the structure shown in Fig. 7(d) has the lowest energy among the six OVCs. However, we also find that the total energy differences between the six $CuIn_5Se_8$ structures are small. With respect to the lowest energy type-*D* structure, the total energy of the type-*A*, type-*B*, type-*C*, type-*E*, and type-*F* structures are only 4, 4, 1, 6, and 8 meV/atom higher, respectively. Similar results are obtained for $CuIn_3Se_5$ as well as for $CuInSe_2$. These results indicate that despite the local environment of OVCs are well defined, containing weighted

TABLE III. Least square fitting results for first shell EXAFS of $CuIn_3Se_5$.

	Coordination number	bond length (Å)	$\Delta\sigma 2$ (Å^2):
Cu-*K* edge	4 ± 0.2	$R_{\text{Cu-Se}}2.424\pm0.005$	$1.4\times10^{-3}+-2\times10^{-4}$
In-*K* edge	4 ± 0.1	$R_{\text{In-Se}}2.595\pm0.005$	$1.4\times10^{-4}+-1\times10^{-5}$

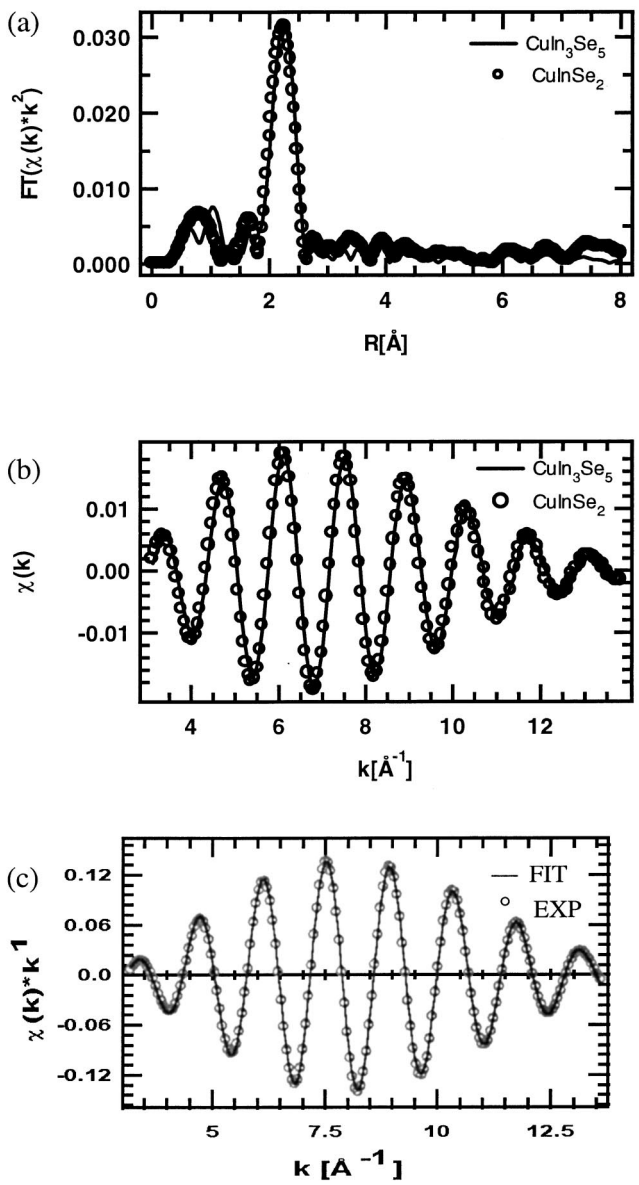

FIG. 3. The In-K edge data for $CuIn_3Se_5$ and $CuInSe_2$. (a) Magnitudes of the Fourier transform, (b) Fourier filtered EXAFS for the first shell peaks, and (c) least-square fits to the Fourier-filtered first shell k^2-weighted $\chi(k)$. The data for $CuIn_3Se_5$ and reference $CuInSe_2$ were filtered over an identical range in r space, from 1.7 to 2.7 Å.

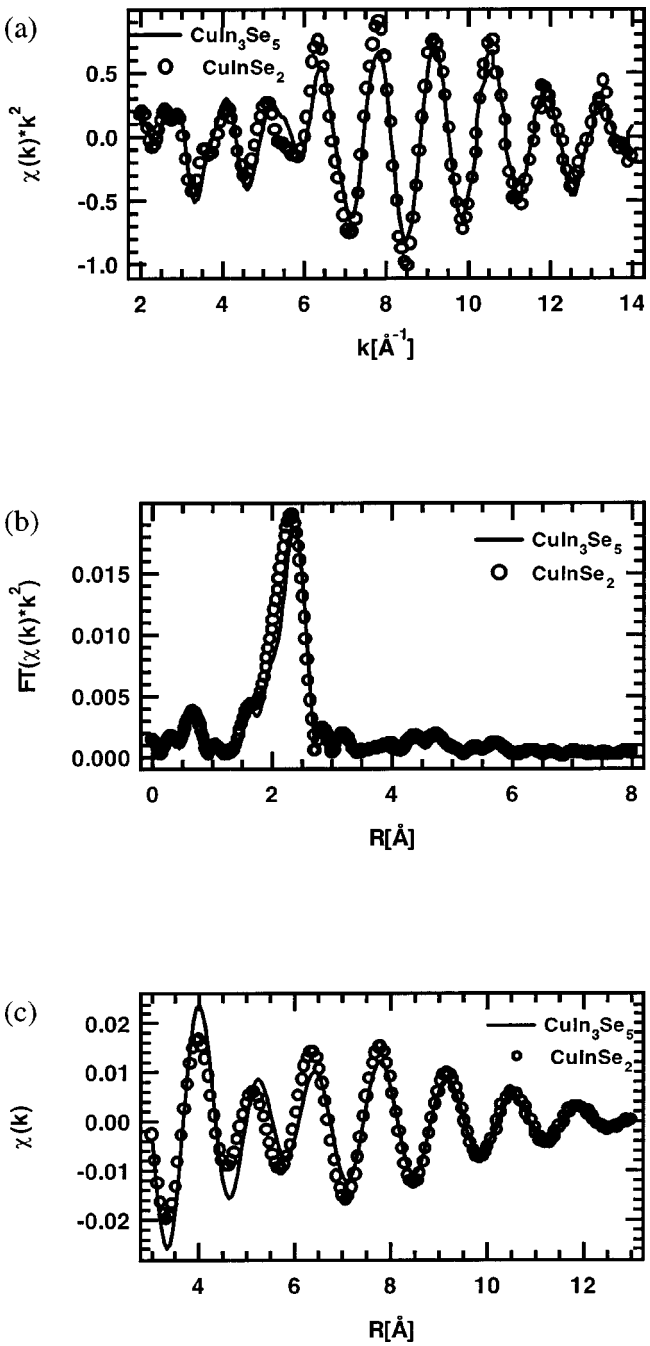

FIG. 4. The Se-K edge for $CuIn_3Se_5$ and $CuIn_3Se_5$. (a) $k^2\chi(k)$ EXAFS spectra, (b) magnitudes of the Fourier transform, and (c) Fourier filtered EXAFS for the first shell peaks.

$k=7$, 8 and 9 clusters, the long range order of the OVCs may depend sensitively on the growth kinetics, the history of the annealing and the configuration entropies. This could explain why different crystal structures of $CuIn_3Se_5$ have been observed.[3–8] For example, the crystal structure proposed by Hanada *et al.*[8] for $CuIn_3Se_5$ has an $I\bar{4}2m$ space group [see Fig. 8(a)]. We find that the model structure of Hanada *et al.*[8] can be described quite well as a superposition of three single phases: (i) 20% of the CA-$CuInSe_2$ [Fig. 8(b)], (ii) 40% of the type-B $CuIn_5Se_8$ [Fig. 8(c)], and (iii) 40% of type-B' $CuIn_5Se_8$ [Fig. 8(d)], where type-B' $CuIn_5Se_8$ is identical to type-B $CuIn_5Se_8$ except that its origin are shifted by $(1/2,1/2,1)a$. The calculated site occupations for the proposed structure are shown in Table V along with the experimental data. We see that the agreement is reasonably good. Similarly, the $CuIn_3Se_5$ model proposed by Nomura's *et al.*[7] can be described as a superposition of CA-$CuInSe_2$ and type-A $CuIn_5Se_8$, and the model proposed by Hönle *et al.*[4] can be approximated as a superposition of P-$CuInSe_2$ and type-F $CuIn_5Se_8$. Our total energy calculation for $CuIn_3Se_5$ shows that the structure model of Hanada *et al.*[8] and Nomura *et al.*[7] have the same total energy, while the structural model of Hönle *et al.*[4] is only about 4 meV/atom higher than the other two models. These results further confirm that the ac-

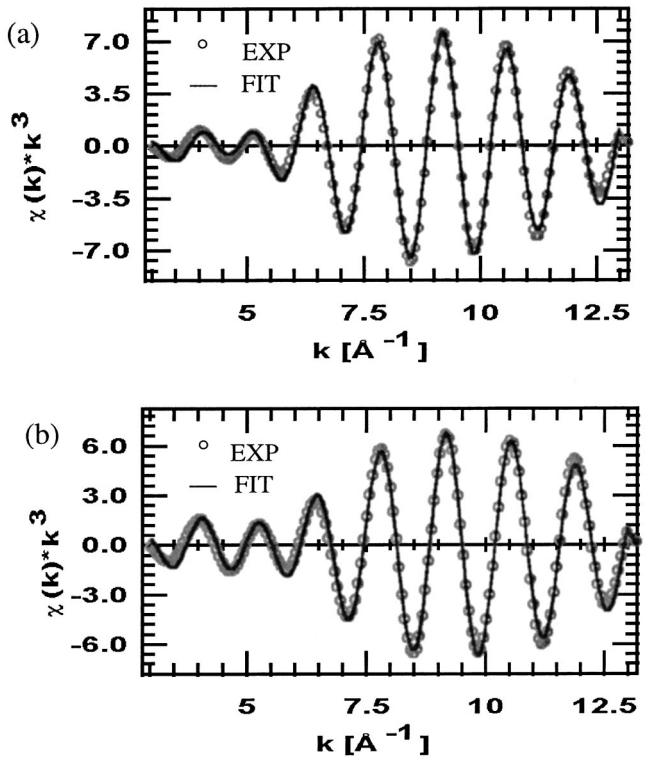

FIG. 5. Least-square fits to the Fourier-filtered first shell Se *K*-edge k^3-weighted $\chi(k)$ data of (a) $CuInSe_2$ and (b) $CuIn_3Se_5$.

tual crystal structure of $CuIn_3Se_5$ depends on the growth conditions.

We have calculated the equilibrium bond lengths in the various OVCs. We find that, within our calculation uncertainty of about 0.005 Å, Cu-Se bond lengths in all these OVCs are independent of the stoichiometry and atomic configurations. For the In-Se bond lengths, we find that it increases linearly with the k number with $R_{\text{In-Se}}(k=9) - R_{\text{In-Se}}(k=7) = 0.06$ Å. However, the averaged In-Se bond lengths are constant within 0.01 Å, decreases slightly as Cu occupation decreases. The theoretical results are consistent with the present EXAFS measurements. The calculated standard deviation for the averaged In-Se bond lengths is around 0.03 Å. To further investigate this problem, temperature dependent EXAFS measurements are required to distinguish the static structural disorder from the thermal disorder.

TABLE IV. EXAFS analysis results for $CuInSe_2$ Se-*K* edge data. FIT indicated fitted parameters.

	$CuInSe_2$	$CuIn_3Se_3$
S_0^2:	0.737 (FIT)	0.737
	Se-Cu	
N:	2	0.8
$R_{\text{Cu-Se}}$ (Å):	2.424	2.424
σ^2 (Å^2):	4.2×10^{-3} (FIT)	1.77×10^{-3} (FIT)
	Se-In	
N:	2	2.4
$R_{\text{In-Se}}$ (Å):	2.598	2.598
σ^2 (Å^2):	4.2×10^{-3} (FIT)	4.22×10^{-3} (FIT)

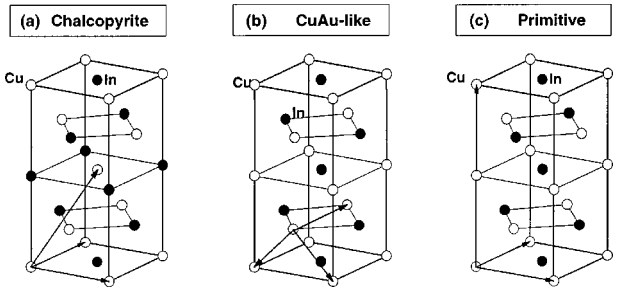

FIG. 6. Crystal structures of $CuInSe_2$: (a) chalcopyrite, (b) CuAu-like, and (c) primitive phases. For clarity the Se atoms are not shown. The lines with arrow give the primitive unit cell lattice vectors for these structures.

IV. DISCUSSIONS

It was found that the Cu and In first nearest neighbor local structures in $CuIn_3Se_5$ are almost identical to those in $CuInSe_2$ with constant average Cu-Se and In-Se bond lengths within 0.01 Å. However, the Se first nearest neighbor local structures in these two compounds are quite different. The least-square fitting of Se *K*-edge EXAFS spectra indicated $CuInSe_2$ was consisted of Se-centered tetrahedron with average two Cu and two In as nearest neighbors. On the other hand, $CuIn_3Se_5$ was consisted of Se-centered tetrahedron with average 0.8 Cu and 2.4 In as nearest neighbors. This result directly proved that $CuIn_3Se_5$ is indeed a defect tetrahedral structure. $CuIn_3Se_5$ can be best described by structures containing weighted local tetrahedral cationic clusters around each Se: $2\text{Cu}+2\text{In}$ $(k=8)$ (20%), and an

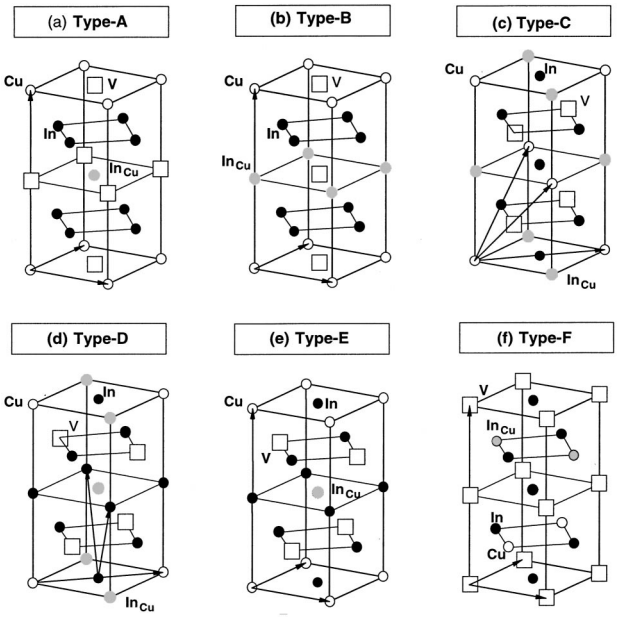

FIG. 7. Crystal structures of $CuIn_5Se_8$: (a) type *A*, (b) type *B*, (c) type *C*, (d) type *D*, (e) type *E*, and (f) type *F*. For clarity the Se atoms are not shown. The lines with arrow give the primitive lattice vectors for these structures.

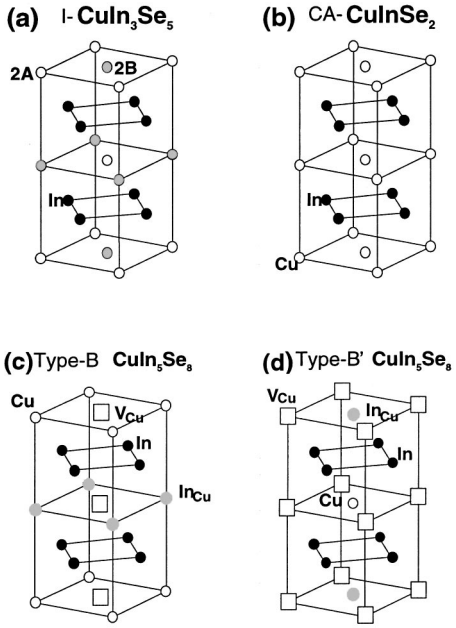

FIG. 8. (a) The proposed crystal structure of $CuIn_3Se_5$ of Hanada *et al.* (Ref. 8). The notations 2*A* and 2*B* etc. indicate different crystallographic sites. (b) The crystal structure of *CA*-$CuInSe_2$. (c) and (d) are the type-*B* and type-*B'* crystal structures of the $CuIn_5Se_8$. The crystal structure in (a) can be considered as supposition of the three crystal structures in (b), (c), and (d). Note that (d) is identical to (c) except that it has a different origin. For clarity the Se atoms are not shown.

equal number (40%) of $V_{Cu}+Cu+2In$ $(k=7)$ and $V_{Cu}+3In$ $(k=9)$, where k denotes the nominal number of valence electrons. The total energy calculations also show that the equilibrium Cu-Se bond lengths in various OVC structures are identical to within the calculation uncertainty (~0.005 Å), and that the In-Se bond lengths in these structures increase linearly with k with $R_{In\text{-}Se}(k=9)-R_{In\text{-}Se}(k=7)=0.06$ Å. The calculations also suggested an equal number of $k=7$ and 9 tetrahedrons. Thus, the average In-Se bond lengths of $CuIn_3Se_5$ would be the same as the In-Se bond length of the $k=8$ tetrahedron. That explains why the average In-Se bond lengths of $CuIn_3Se_5$ and $CuInSe_2$ are the same, since $CuInSe_2$ consists of only $k=8$ tetrahedrons. It is revealing to compare the structure models proposed in the literature with EXAFS data. The structure solution ($P\bar{4}2c$) proposed by Hönle *et al.*[4] is given in Fig. 9(a) with a $M2$-Se bond length of 2.42 Å and an In-Se bond length around 2.615 Å. $M2$ was assigned to Cu atoms and vacancies based on the bond length value. The bond lengths of the $M1$-Se and $M3$-Se pairs are around 2.47 Å, and the $M1$ and $M3$ sites are mainly occupied by In atoms and vacancies. The short In-Se bond lengths were explained through a vacancy influenced relaxation mechanism. The model proposed by Hanada *et al.*[8] is given in Fig. 9(b). This structure model will produce both Cu-Se and In-Se bond lengths of equal value (2.49 Å). In addition, the assigned Se position could not reproduce the powder XRD pattern, especially the 101 reflection. The Se position would have to move from the ideal zinc-blende position to produce the 101 reflection at similar magnitude. Merino *et al.*[9] refined Hanada's $I\bar{4}2m$ structure model using powder XRD data. Their structure model will produce Cu-Se bond lengths of 2.657 and 2.273 Å for $Cu_2In_4Se_7$ and $CuIn_3Se_5$, respectively, and In-Se bond lengths of 2.239 and 2.563 Å for $Cu_2In_4Se_7$, and 2.676 and 2.529 Å for $CuIn_3Se_5$. None of these bond length values are consistent with current EXAFS data. This discrepancy may be explained by considering the differences in the two characterization techniques.

TABLE V. Comparison of atomic site occupations of the model proposed by Hanada *et al.* (Ref. 8) for $CuIn_3Se_5$ and the superposition model of present theory which treat it as a linear combination of 20% *CA*-$CuInSe_2$, 40% of type-*B* $CuIn_5Se_8$, and 40% of type-*B'* $CuIn_5Se_8$ (Fig. 15).

Site	Calc. occupation	Expt. occupation
2*A*	0.6 Cu	0.8 Cu
2*B*	0.2 Cu+0.4 In	0.4 In
In	1.0 In	1.0 In
Se	1.0 Se	1.0 Se

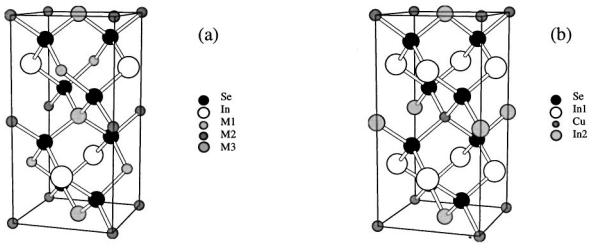

Space Group: $P\bar{4}2c$

Se	8n (0.2575, 0.2353, 0.1178)	0.9
In	2d (0, 1/2, 1/4)	1
M1	2b (1/2, 0, 1/4)	0.57 (In) 0.02 (Cu)
M2	2e (0,0,0)	0.68 (Cu)
M3	2f (1/2, 1/2, 0)	0.6 (In) 0.02 (Cu)

Space Group: $I\bar{4}2m$

Se	8i (1/4, 1/4, 1/8)	1
In1	4d (0,1/2, 1/4)	1
In2	2b (0, 0, 1/2)	0.4
Cu	2a (0, 0, 0)	0.8

FIG. 9. (a) The $P\bar{4}2c$ structure model and solution proposed by Hönle *et al.* (Ref. 4). (b) The $I\bar{4}2m$ structure model and solution proposed by Hanada *et al.* (Ref. 8).

XRD determines the distance between crystallographic sites. In contrast, EXAFS measures the average local structure around a specific type of atom, including inter-atomic distances. It is clear that the local structures of these crystals are well defined based on the EXAFS data and first-principles calculations, however, the long-range order structure is not. This is clearly evident from examining the various structure solutions for $CuIn_3Se_5$. All structure solutions have cation sites shared by Cu, In, and the vacancy in varying degrees. For example, In shared $M1$ and $M3$ sites with Cu and a vacancy in Hönle *et al.*'s[4] model. $M1$-Se and $M3$-Se distances are actually an average of In-Se, Cu-Se, and vacancy-Se distances. Furthermore, the disorder in the cation sublattice also lead to a displacement of the Se atoms from its crystallographic site position to maintain the equilibrium bond distance according to its local environment. This observation is consistent with the vacancy relaxation mechanism proposed by Hönle *et al.*[4] This anion displace-

ment phenomenon could also explain the lower occupancy number reported for Se atoms in Hönle *et al.*[4] A similar vacancy-induced atomic relaxation was also observed in the ordered vacancy compound $CdIn_2Se_4$. Bernard and Zunger[25] showed that Se atoms move toward the vacancy and maintain the ideal tetrahedral bond lengths of Cd-Se and In-Se in $CdIn_2Se_4$.

One difficulty associated with determining the structure of these compounds is identifying the symmetry. As suggested by the EXAFS and XRD data, the Se atoms do not occupy the assigned atomic positions based on one space group symmetry. Rather, the system maintains a short-range order and the anion always displaces in a way to reserve the equilibrium Cu-Se and In-Se bond lengths. The long-range order, which gives the superlattice peaks, is not uniquely determined in this system because many structures have very similar total energies based on first principle calculations. This could explain why very different electron diffraction patterns were reported for $CuIn_3Se_5$.[6,8]

V. SUMMARY

We have studied the crystal structure of $CuInSe_2$ and $CuIn_3Se_5$ using EXAFS measurements and first-principles total energy calculations. We find that the Cu and In first nearest neighbor local structures in $CuIn_3Se_5$ are almost identical to those in $CuInSe_2$. However, the Se first nearest neighbor local structures are different. In $CuInSe_2$ Se has two Cu and two In as nearest neighbors. On the other hand, in $CuIn_3Se_5$ Se has in average 0.8 Cu and 2.4 In as nearest neighbors. These results directly proved that $CuIn_3Se_5$ is indeed a defect tetrahedral structure. The local structure of $CuIn_3Se_5$ is well defined. It can be best described by structures containing 20% $k=8$ (2Cu+2In), and 40% each of $k=7$ (V_{Cu}+Cu+2In) and $k=9$ (V_{Cu}+3In) clusters around each Se. From the EXAFS analysis, we have found the average Cu-Se and In-Se bond lengths are the same for $CuInSe_2$ and $CuIn_3Se_5$. This is in contrary to all published structural models for $CuIn_3Se_5$. First-principles total energy calculations were also performed to help elucidate this discrepancy. The calculations indicate that the equilibrium Cu-Se bond lengths are the same in various OVCs. The equilibrium In-Se bond lengths increase slightly with k, but the averaged In-Se bond lengths are the same for $CuIn_3Se_5$ and $CuInSe_2$, within 0.01 Å. The discrepancy on the bond lengths between present results and early studies are explained through cation and anion sites disorder. Finally, we show that the formation energies of various crystal structures for $CuIn_3Se_5$ are very similar. This could explain why different crystal structures of this In-rich compound have been observed.

ACKNOWLEDGMENTS

The work at NREL was supported by the U.S. Department of Energy, under Contract No. DE-AC36-98-GO10337. The work at the University of Florida was supported by the DOE/NREL Thin Film PV Partnership Program under Subcontract No. XAF-5-14142-10. The MRCAT beamline is supported by the U.S. DOE BES and member institutions. Travel for J.W.J. and C.H.C. was supported by a University of Florida DSR Opportunity Fund grant. Use of the Advanced Photon Source was supported by the U.S. Department of Energy, Office of Science, Basic Energy Sciences Division, under Contract No. W-31-109-Eng-38.

*Electronic address: changch@che.orst.edu

[1] M. Contreras, B. Egaas, K. Ramanathan, J. Hiltner, A. Swartzlander, F. Hasoon, and R. Noufi, Prog. Photovoltaics **7**, 311 (1999).
[2] D. Schmid, M. Ruckh, F. Grunwald, and H. W. Schock, J. Appl. Phys. **73**, 2902 (1992).
[3] L. S. Palatnik and E. J. Rogacheva, Dokl. Akad. Nauk SSSR **174**, 80 (1967) [Sov. Phys. Dokl. **12**, 502 (1967)].
[4] W. Hönle, G. Kühn, and U.-C. Boehnke, Cryst. Res. Technol. **23**, 1347 (1988).
[5] B. H. Tseng and C. A. Wert, J. Appl. Phys. **65**, 2254 (1989).
[6] H. Z. Xiao, L.-Chung Yang, and A. Rockett, J. Appl. Phys. **76**, 1503 (1994).
[7] S. Normura and S. Endo, Trans. MRS Jpn **20**, 755 (1996).
[8] T. Hanada, A. Yamana, Y. Nakamura, O. Nittono, and T. Wada, Jpn. J. Appl. Phys. **36**, L1494 (1997).
[9] J. M. Merino, S. Mahanty, M. Leon, R. Diaz, F. Rueda, and J. L. Martin de Vidales, Thin Solid Films **361–362**, 70 (2000).
[10] S. B. Zhang, S.-H. Wei, and A. Zunger, Phys. Rev. Lett. **78**, 4059 (1997).
[11] S. B. Zhang, S.-H. Wei, A. Zunger, and H. Katayama-Yoshida, Phys. Rev. B **57**, 9642 (1998).
[12] Z. A. Shukri, C. H. Champness, and I. Shih, J. Cryst. Growth **129**, 107 (1993).
[13] D. Sayers and B. Bunker, in *X-Ray Absorption: Principles, Application, Techniques of EXAFS, SEXAFS, and XANES*, edited by D. C. Koningsberger and R. Prins (Wiley, New York, 1987), Chap. 6.
[14] T. Ressler, J. Phys. IV **7**, C2-269 (1997).
[15] A. L. Ankudinov and J. J. Rehr, Phys. Rev. B **52**, 2995 (1995).
[16] J. Parkes, R. D. Tomlinson, and M. J. Hampshire, J. Appl. Crystallogr. **6**, 414 (1973).
[17] H. W. Spiess, U. Haeberln, G. Brandt, A. Räuber, and J. Schneider, Phys. Status Solidi B **62**, 183 (1974).
[18] G. Zahn and P. Paufler, Cryst. Res. Technol. **23**, 499 (1988).
[19] K. S. Knight, Mater. Res. Bull. **27**, 161 (1992).
[20] J. M. Merino, J. L. Martin de Vidales, S. Mahanty, R. Diaz, and F. Rueda, J. Appl. Phys. **80**, 5610 (1996).
[21] F. Frolow, L. Chernyak, D. Cahen, H. Hallak, J. Gabboun, A. Kvick, and H. Graafama, Inst. Phys. Conf. Ser. **152**, 67 (1998).
[22] C.-H. Chang, S.-H. Wei, J. W. Johnson, R. N. Bhattacharya, B. J. Stanbery, T. J. Anderson, and R. Duran, Jpn. J. Appl. Phys., Suppl. **39-1**, 411 (2000).
[23] E. Parthé, *Crystal Chemistry of Tetrahedral Structures* (Gordon and Breach, New York, 1964).
[24] S.-H. Wei and H. Krakauer, Phys. Rev. Lett. **55**, 1200 (1985), and references therein.
[25] J. E. Bernard and A. Zunger, Phys. Rev. B **37**, 6835 (1988).